Characterization of rapidly consolidated γ-TiAl

Kunal Kothari[1a], Ramachandran Radhakrishnan[1b], Tirumalai S. Sudarshan[2c]
and Norman M. Wereley*[1]

*[1]Composites Research Laboratory, Department of Aerospace Engineering,
University of Maryland, College Park, MD 20742, USA*
[2]Materials Modification Inc., Fairfax, VA 22031, USA

Abstract. A powder metallurgy-based rapid consolidation technique, Plasma Pressure Compaction (P²C®), was utilized to produce near-net shape parts of gamma titanium aluminides (γ-TiAl). Micron-sized γ-TiAl powders, composed of Ti-50%Al and Ti-48%Al-2%Cr-2%Nb (at%), were rapidly consolidated to form near-net shape γ-TiAl parts in the form of 1.0" (25.4 mm) diameter discs, as well as 3"×2.25" (76.2 mm × 57.2 mm) tiles, having a thickness of 0.25" (6.35 mm). The γ-TiAl parts were consolidated to near theoretical density. The microstructural morphology of the consolidated parts was found to vary with consolidation conditions. Mechanical properties exhibited a strong dependence on microstructural morphology and grain size. Because of the rapid consolidation process used here, grain growth during consolidation was minimal, which in turn led to enhanced mechanical properties. Consolidated γ-TiAl samples corresponding to Ti-48%Al-2%Cr-2%Nb composition with a duplex microstructure (with an average grain size of 5 μm) exhibited superior mechanical properties. Flexural strength, ductility, elastic modulus and fracture toughness for these samples were as high as 1238 MPa, 2.3%, 154.58 GPa and 17.95 MPa m$^{1/2}$, respectively. The high temperature mechanical properties of the consolidated γ-TiAl samples were characterized in air and vacuum and were found to retain flexural strength and elastic modulus for temperatures up to 700ºC. At high temperatures, the flexural strength of γ-TiAl samples with Ti-50%Al composition deteriorated in air by 10% as compared to that in vacuum. γ-TiAl samples with Ti-48%Al-2%Nb-2%Cr composition exhibited better if not equal flexural strength in air than in vacuum at high temperatures.

Keywords: intermetallics; grain size; rapid consolidation; titanium aluminide; powder metallurgy

1. Introduction

Dual phase gamma titanium aluminides (γ-TiAl) have attracted significant attention in the last twenty years for properties that enable high temperature automotive and aerospace applications (Das *et al.* 2004, Djanarthany *et al.* 2001, Immarigeon *et al.* 1995, Froes *et al.* 1992, Voice 1999). One of the foremost applications for which γ-TiAl has been considered is in high performance gas turbine engines (Krause *et al.* 1999). Due to its high specific strength, γ-TiAl alloys have become leading

candidates to replace Ni-based superalloys in gas turbine engines. Replacement of Ni-based superalloys parts with titanium aluminides is expected to reduce the structural weight of high performance gas turbine engines by as much as 20-30% (Voice *et al.* 2005). Hence, a significant increase in engine efficiency and performance is expected with use of γ-TiAl in gas turbine engines.

Titanium aluminides display attractive properties such as high specific strength, high stiffness and good corrosion, creep, and oxidation resistance. Due to their long order nature they lack room temperature ductility and fracture toughness. Fatigue crack growth rates are also an area of concern (Soboyejo *et al.* 1997, Soboyejo *et al.* 2004). For a long time, the attractive properties of γ-TiAl were outweighed by their difficulty in processing and machining at room temperature. But advances in manufacturing technologies, deeper understanding of the microstructure of titanium aluminides, deformation mechanisms, and advances in micro-alloying, have led to first commercial uses of titanium aluminides in high performance turbochargers for Formula One and sports cars (Sommer and Keijzers 2003).

Popular techniques that have been used to produce γ-TiAl parts include: investment casting, ingot metallurgy (IM), and powder metallurgy (PM). More recently advanced techniques such as direct rolling, laser forming, and mechanical alloying have been investigated with good success. Several rapid sintering/consolidation techniques such as spark plasma sintering, pulse discharge sintering and explosive consolidation have also been successful in forming TiAl with the desired mechanical properties (Chen *et al.* 2009, Szewczak *et al.* 1997, Cheng and McLean 1997, Fu *et al.* 2001, Hitoshi and Sun 2003, Lu *et al.* 2009).

Superalloys have tensile strength in the range of 1.2 GPa with a 3-5% elongation before failure. γ-MET TiAl alloys (Draper *et al.* 2003, Shazly *et al.* 2009) with small additions of Nb, Cr, and B have matched the strength of Ni-based superalloys. Small additions of Cr have improved the room temperature ductility of γ-TiAl (Kim 1989, 1991, Marketz *et al.* 2002), while Nb additions have been reported to improve high temperature strength retention and oxidation resistance (Appel *et al.* 2000, Christop *et al.* 1997, Gerling *et al.* 2004). Additions of B have aided in grain refinement and increased strength of γ-TiAl (Sahay *et al.* 1999).

A key drawback of γ-TiAl is its production cost as compared to that of Ni-based superalloys. The cost differential is largely a result of processing techniques because materials with fairly low ductility are extremely problematic. Further, due to the long-range ordering of γ-TiAl up to its melting point, processing temperatures are fairly high. This requires capital investment in processing equipment with good high temperature control characteristics.

Investment casting, ingot metallurgy and powder metallurgy techniques have been successful at producing γ-TiAl parts with desirable mechanical properties only after a series of post processing steps, like hot-isostatic pressing, ageing, annealing, and hot working (Draper *et al.* 2003, Zhang *et al.* 2011). These steps further add to the production cost of TiAl and also require exposure to high temperatures for long periods of time. This in turn leads to grain growth and deterioration of strength as confirmed by the Hall-Petch relationship for γ-TiAl (Soboyejo *et al.* 2004).

Powder metallurgy (PM) offers the potential for minimizing many of the problems associated with large ingot production and reducing the overall cost of the final γ-TiAl component. Many of the problems associated with ingot metallurgy (IM), such as centerline porosity, chemical inhomogeniety, regions of varying density and microstructure can be solved by PM. Further, PM enables the development of new alloys that cannot be made by conventional IM (Yolton *et al.* 2003).

Hence, a PM-based rapid consolidation technique is required to produce γ-TiAl parts with minimal grain growth, minimal post-processing steps, and desired microstructure with enhanced mechanical properties. In this study, a novel rapid consolidation technique, Plasma Pressure
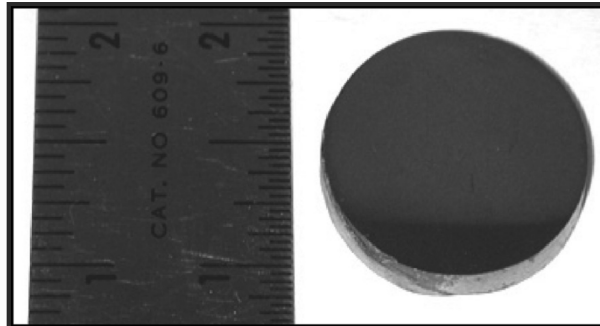
Fig. 1 P^{2}C$^®$ consolidated Ti-50%Al disc
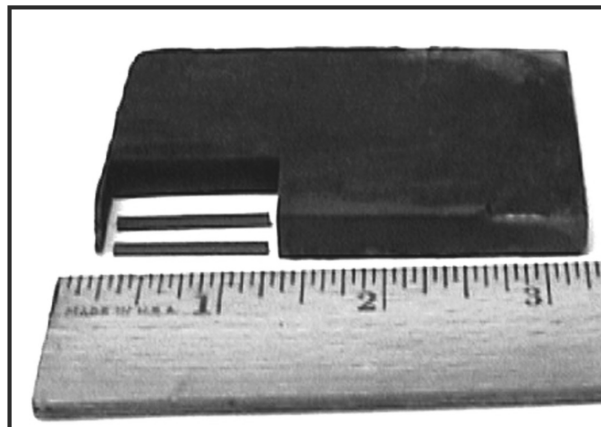
Fig. 2 P^{2}C$^®$ consolidated Ti-50%Al tile

Compaction (P^{2}C$^®$), developed by Materials Modification, Inc. (Fairfax, VA, USA) was utilized to consolidate commercially available γ-TiAl powders. The objective of this study was to produce fully dense near-net shape parts of γ-TiAl via P^{2}C$^®$ with minimal grain growth and the desired microstructure. A further aim of this study was to consolidate γ-TiAl powders with small additions of Nb and Cr to enhance ductility and high temperature strength.

2. Experimental procedure

-325 mesh (<45 μm) γ-TiAl powders with composition of Ti-50%Al and Ti-48%Al-2%Cr-2%Nb (at%)[1] were procured from commercial vendors. Ti-50%Al (at%) powders were procured from CERAC, Milwaukee, WI and ESPI, Inc., Ashland, OR, USA. The Ti-48%Al-2%Cr-2%Nb composition powders were procured from Crucible Research, Pittsburgh, PA, USA, respectively.

The powders were consolidated using the P^{2}C$^®$ process. The powders with Ti-50%Al composition

---

[1]All the elemental concentrations mentioned henceforth will be in at%, unless specified otherwise
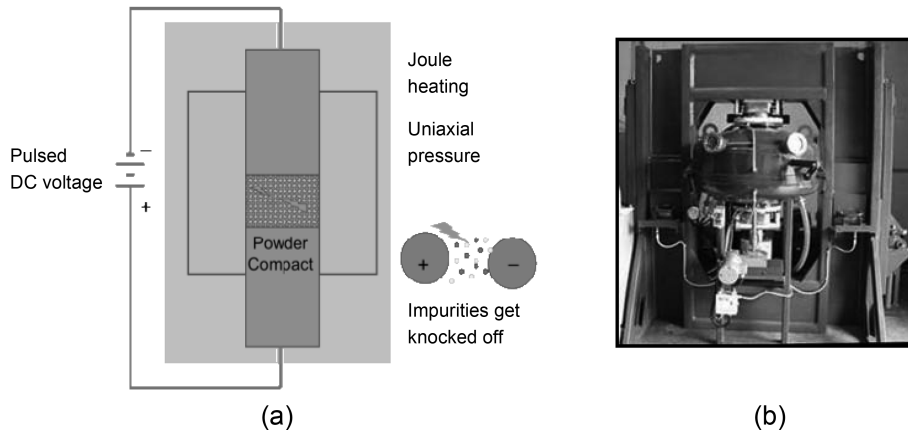
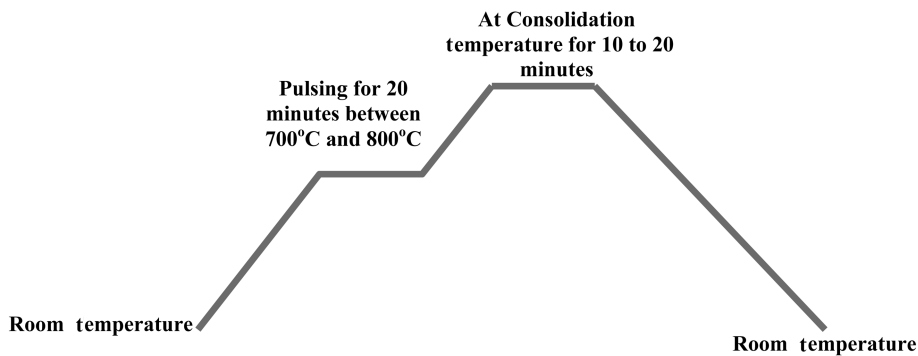Fig. 3 Plasma pressure compaction process (a) illustration, and (b) set-up

Fig. 4 Consolidation profile for plasma pressure compaction ($P^2C^®$)

were consolidated into 1" (25.4 mm) diameter disks and 3"×2.25" (76.2 mm×57.2 mm) tiles, both having thickness of 0.25" (6.35 mm), as shown in Fig. 1 and Fig. 2. The Ti-48%Al-2%Cr-2%Nb powders were consolidated into 3"×2.25"×0.25" (76.2 mm× 57.2 mm×6.35 mm) tiles.

2.1 Plasma pressure compaction

During consolidation, γ-TiAl powders were placed in a graphite die with plungers inserted on both sides. This assembly was then placed between water-cooled electrodes and the chamber containing this assembly was evacuated. The lower electrode was raised using a hydraulic cylinder to hold the entire assembly together in compression and provide a path for current to flow. When sufficient inter-particle contact was established by applying uniaxial pressure, pulsed DC voltage was applied through the powder compact using a full-wave-rectified power supply.

Pulsed electrical power was applied with high current at an adequate voltage. This leads to charge build up at inter-particle gaps. This causes one particle to be charged negatively with respect to another particle that is in contact with it. As the charge accumulates, the voltage difference becomes sufficiently large to generate sparks that trigger an ionization process. The ions move towards the

Table 1 Consolidation conditions for γ-TiAl samples consolidated by P^{2}C$^®$

Sample ID	Powder composition (at%)	Consolidation time (Minutes)	Consolidation pressure (MPa)	Temperature (Celsius)	P^{2}C$^®$ pulsing	Cooling rate (K/min)
S1[*]	Ti-50%Al	20	54	T_α - 235 (1200)	Yes	60
S2	Ti-50%Al	10	54	T_α - 435 (1000)	Yes	60
S3	Ti-50%Al	10	54	T_α - 435 (1000)	No	60
S4	Ti-50%Al	10	54	T_α - 235 (1200)	Yes	60
S5	Ti-50%Al	10	54	T_α - 235 (1200)	No	60
S6	Ti-50%Al	20	54	T_α - 35 (1400)	Yes	60
T1	Ti-50%Al	20	30	T_α - 435 (1000)	Yes	200
T2	Ti-50%Al	20	30	T_α - 435 (1000)	Yes	60
T3[**]	Ti-48%Al-2%Cr-2%Nb	20	30	T_α - 145 (1200)	Yes	60
T4[**]	Ti-48%Al-2%Cr-2%Nb	20	30	T_α + 55 (1400)	Yes	60

Note: Sample IDs with 'T' prefix are tiles and with 'S' prefix are discs.
All powders procured from ESPI, Inc., Ashland, OR, unless indicated otherwise.
[*]Powders Procured from CERAC, Milwauke, WI, USA.
[**]Powders Procured from Crucible Research, Pittsburgh, PA, USA.

negatively charged particles while the electrons move toward the positively charged particles. The ionization process occurs in the form of sparks or plasma generation depending on the energy level at the inter-particle gap. The formation of plasma removes surface oxides and other contaminants, which form a diffusion barrier in the consolidation process. As a result, particle re-arrangement and diffusion is enhanced. After pulsing, direct current was applied through the powder compact resulting in Joule heating as shown in Fig. 3(a).

Fig. 4 shows the consolidation profile for the P^{2}C$^®$ process. Pulsing was performed between 700°C and 800°C for about 20 minutes. The P^{2}C$^®$ profile for γ-TiAl was selected based on the binary Ti-Al phase diagram as shown in Fig. 5, as well as data from the literature (Kim 1989, 1991). The P^{2}C$^®$ consolidation conditions are discussed below.

2.2 P^{2}C$^®$ Consolidation conditions

The P^{2}C$^®$ consolidation conditions for all the samples are listed in Table 1. The samples were consolidated at temperatures in the $\alpha_2 + \gamma$, $\alpha + \gamma$ and α phase fields (Fig. 5). The consolidation pressure was set to be in the range of 30 MPa to 54 MPa. All of the phase field temperatures were determined using the binary phase diagram (Fig. 5). The $\alpha_2 + \gamma$ phase field boundary was determined to be close to 1200°C, while the $\alpha + \gamma$ phase field boundary or the α-transus temperature (T_α) of the Ti-50%Al composition was determined to be close to 1435°C. The alpha-transus temperature for Ti-48%Al-2%Cr-2%Nb composition was determined to be 1345°C. Consolidation was conducted in vacuum at temperatures ranging from 1000°C (T_a - 435°C) to 1400°C (T_a - 35°C), as indicated in Fig. 5.

Along with temperature, consolidation parameters such as pulsing, and cooling rate were also varied. Most of the samples were consolidated with the application of the pulsing process. For comparison purposes, two of the 1" diameter discs of Ti-50%Al composition (samples S3 and S5) were consolidated without the application of the pulsing process. During the P^{2}C$^®$ process, different
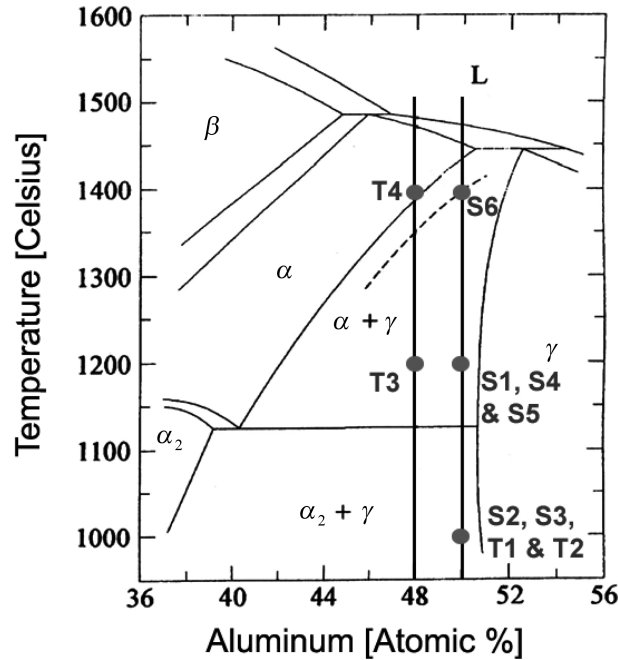
Fig. 5. Partial Ti-Al binary phase diagram near the stoichiometric γ-TiAl composition indicating consolidation
temperatures (Rivard 2005)

cooling rates were used to cool the tiles from their consolidation temperature to room temperature. This was achieved by controlling the DC voltage applied to the sample. The cooling rate for most of the P^{2}C$^®$ consolidated samples was set to 60 K/min. For one of the Ti-50%Al tiles (sample T1), cooling rate was accelerated to 200 K/min.

2.3 Microscopy

The consolidated samples were sectioned and metallographically polished to a 1 μm diamond finish. They were subsequently etched using Kroll's reagent. Their microstructure was characterized via Scanning Electron Microscopy (SEM) and Energy Dispersive Spectroscopy (EDS). The SEM micrographs were taken in an orientation perpendicular to the direction of compaction.

2.4 Mechanical tests

Mechanical properties of the consolidated specimens were characterized using four-point bending tests. A self-aligning silicon carbide four-point bending fixture was designed according to ASTM standard C1161 (ASTM 1997) with an outer-span of 20 mm and an inner-span of 10 mm. Consolidated samples were machined with chamfered edges to a dimension of 25 mm $\times$ 1.5 mm $\times$ 2.0 mm. Samples with dimension of 3 mm $\times$ 4 mm $\times$ 25 mm with a 60 degree chevron notch were also tested according to ASTM standard C1421 in the four-point bending set-up to measure fracture toughness.

All tests were conducted at a strain rate of 0.75×10^{-4} in a servohydraulic testing machine

(Material Testing Systems, model 810). The four-point bending tests were conducted at temperatures up to 950°C. The high temperature tests were conducted in air, as well as vacuum (10^{-5} Pa). Test samples were loaded in the four-point bending test fixture, such that the resultant tensile and compressive stresses were in the direction perpendicular to that of the direction of the compaction.

For four-point bending tests performed at room temperature, bend bars were mounted with strain gages on the side under pure tension. The strain data, along with load and displacement data, was used to calculate the elastic modulus of the material, as well as elongation and flexural strength. The stress (σ) along the span and the thickness of the bend bar was calculated using the flexure formula (Hibbeler 1997).

To ensure the accuracy of the results obtained by four-point bending, control samples prepared from AD998 aluminum oxide obtained from CoorsTek, Golden, CO were also tested. The flexure strength, fracture toughness and Young's modulus of the AD998 samples were in excellent agreement with those reported by CoorsTek.

For high temperature four-point bending tests, strain gages could not be mounted on the specimens due to the operational temperature limit of the strain gages. Instead, at high temperatures, the elastic modulus in bending was calculated using the load and displacement data collected from the built-in load cell and displacement sensor of the MTS 810 load frame.

High temperature four-point bending tests were performed in both air and vacuum. For high temperature tests in vacuum, the four-point bending test set-up was enclosed in a retort with a bellows assembly. The bellows assembly was used on the top and bottom of the retort to provide a seal at the loading rods. A diffusion vacuum pump was used to obtain vacuum in the range of 10^{-5} Pa.

The density of the consolidated samples was determined using the immersion method (Archimedes' principle) on precisely Electro-Discharge Machined (EDM) specimens used for four-point bending tests. Micro-hardness of the consolidated samples was obtained on polished specimens using a diamond Vickers indent under a load of 1000 grams with a dwell time of 15 seconds.

3. Results

3.1 Density

The theoretical density of pure γ-TiAl phase is 3.76 gm/cm^3, while that of the α_2-Ti$_3$Al phase is 4.1 gm/cm^3 (Sauthoff 1995). Except for samples T1 and T2, the density of the consolidated samples was found to be in the range of 3.8~4 gm/cm^3 as shown in Fig. 6. The density values of the specimens are between the theoretical values of γ-TiAl and α_2-Ti$_3$Al, which indicates the presence of both γ-TiAl and α_2-Ti$_3$Al phases.

The density of the Ti-50%Al tile specimens T1 and T2 was found to be lower than the theoretical density of γ (TiAl) phase. This indicates that the tile specimens T1 and T2 may not have been fully densified. This was further confirmed by microscopy below.

3.2 Microscopy

The SEM micrograph of sample S1 in Figs. 7 and 8 shows the presence of two different phases as seen by the color contrast. To determine the chemical composition of the different phases present in
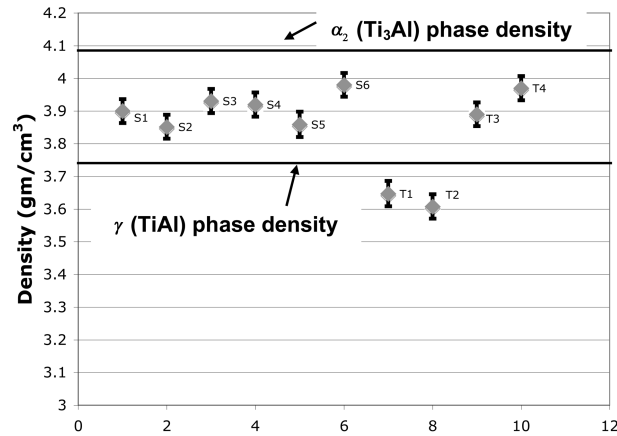
Fig. 6 Density of $P^2C^®$ consolidated γ-TiAl samples
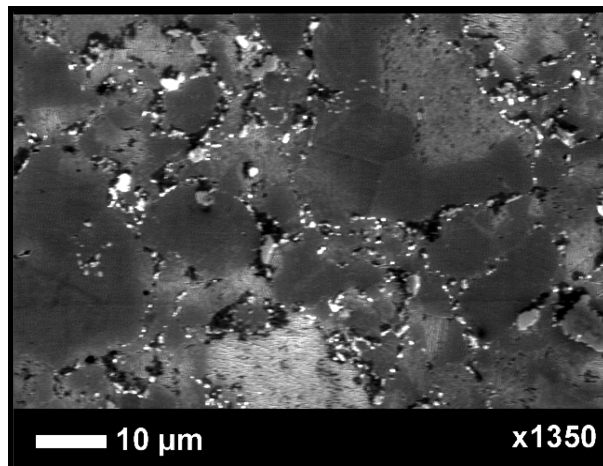
Fig. 7 Scanning electron micrograph of $P^2C^®$ consolidated Ti-50%Al sample - S1

sample S1, Energy Dispersive Spectroscopy (EDS) was performed. EDS revealed the presence of γ (TiAl) phase as the dark phase and α_2 (Ti$_3$Al) phase as the lighter phase as shown in Fig. 8. The α_2 (Ti$_3$Al) phase was segregated at the grain boundaries. The fine alternating dark and light structures in the grains in Fig. 8 were determined by EDS to be alternating plates of α_2 (Ti$_3$Al) and γ (TiAl) phase. Based on published literature (Kim 1989, 1991, 1995, 1998, Kim and Dimiduk 1991), the microstructure was determined to be near gamma/duplex. The microstructure consisted of large gamma grains, small equiaxed gamma grains and lamellar colonies. The EDS performed on sample S1 also revealed pockets of high concentration of Oxygen as indicated by the dark black areas in Fig. 7.

The SEM micrographs of samples S2, S3, S4, S5, and S6 are shown in Fig. 9. All of these samples were consolidated into one-inch diameter discs from Ti-50%Al powders procured from the same vendor. As shown in Fig. 9, the microstructure of samples S2 to S6 exhibited a range of features. These features are characteristic of γ-TiAl as discussed below.
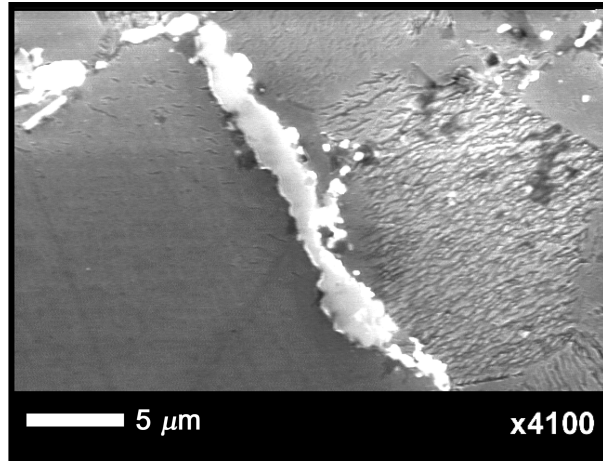
Fig. 8 SEM micrograph of P^{2}C$^®$ consolidated sample S1 showing α_2-Ti$_3$Al phase (light phase), γ-TiAl phase (dark phase) and a lamellar colony with alternating plates of α_2-Ti$_3$Al and γ-TiAl

SEM micrographs of sample S2 are shown in Fig. 9(a). Correlating the microstructure of S2 with its EDS analysis, its microstructure was found to consist of large and small gamma grains. The α_2 (Ti$_3$Al) phase was segregated at the grain boundaries. This is characteristic of a near gamma microstructure. The average grain size as determined using the line-intercept method was 10 μm. The dark black areas in the SEM micrographs of sample S2 were found to contain oxygen and carbon impurities.

Sample S3 was consolidated at the same conditions as sample S2 except that the pulsing process was not applied during consolidation. The SEM micrographs of sample S3 (Fig. 9(b)) exhibited similar characteristics to that of sample S2, except that SEM of S3 exhibited higher concentration of small black areas as compared to that of S2. As mentioned earlier EDS revealed high concentration of oxygen and carbon in the small dark areas. The average grain size of sample S3 was determined to be 10 μm, similar to that of sample S2.

SEM micrographs of samples S4 revealed a microstructure consisting of large and equiaxed gamma grains and pockets of lamellar colonies as shown in Fig. 9(c). Few precipitates of α_2 (Ti$_3$Al) were segregated at the grain boundaries. This was found to be characteristic of the near gamma and duplex microstructure. The average grain size as determined from the line-intercept method was found to be 13 μm. The dark black areas in the SEM micrographs of sample S4 in Fig. 9(c) were analyzed by EDS and found to contain oxygen and carbon.

Sample S5 was consolidated at the same conditions as sample S4, except that it was not subjected to pulsing. The SEM micrographs of sample S5 in Fig. 9(d) showed similar characteristics to that of sample S4. The average grain size of sample S5 was determined to be 13 μm.

The SEM micrographs of sample S6 shown in Fig. 9(e) reveal the presence of lamellar colonies made up of alternating α_2 and γ plates. The average size of the lamellar colonies was found to be in the range of 75 micrometers. The microstructure was characterized as fully lamellar. The average thickness of lamellae was found to be 1 μm.

The SEM micrographs of the two tiles T1 and T2 with Ti-50%Al composition are shown in Figs. 10(a) and 10(b). The microstructure of T1 and T2 was similar with a mix of large and small gamma
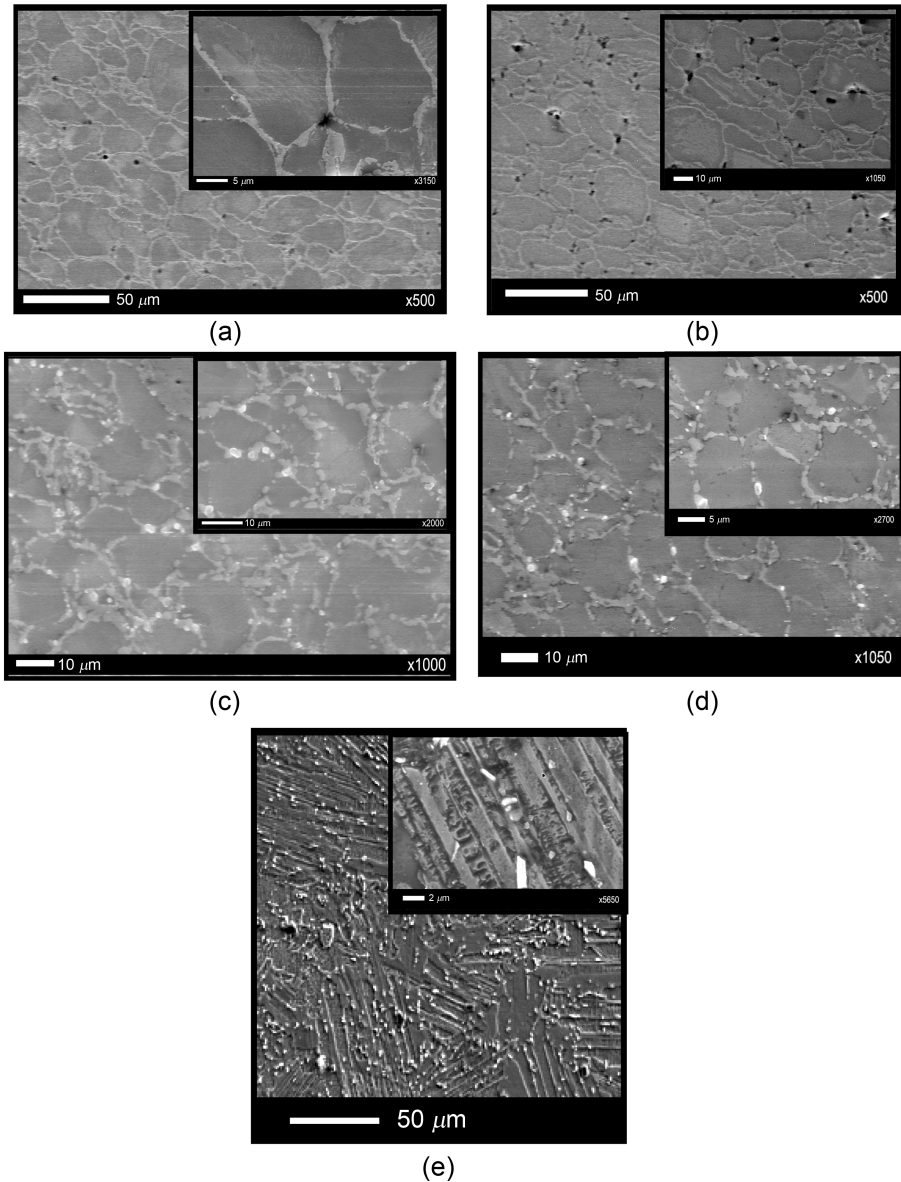
Fig. 9 SEM of Ti-50%Al disc samples (a) S2 – near gamma, (b) S3 – near gamma, (c) S4 – near gamma/duplex, (d) near gamma/duplex and (e) S6 – fully lamellar

grains. The dark areas were identified to be γ (TiAl) phase, while the light areas were identified as α_2 (Ti$_3$Al) phase by EDS. Both the microstructures were observed to have dark black areas at the grain boundaries. The EDS analysis revealed presence of oxygen and carbon impurities, and pores in the dark black areas. The presence of significant volume of pores was further confirmed by density measurements. The density of both the tile samples was much lower than that of α_2 (Ti$_3$Al) and γ (TiAl) phases. The average grain size of T1 and T2 as determined by the line-intercept method was 10 μm.

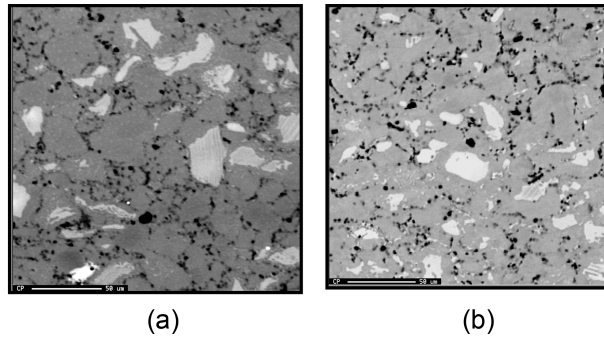(a)   (b)

Fig. 10 SEM of P^{2}C$^®$ consolidated Ti-50%Al tiles (a) sample T1, and (b) sample T2
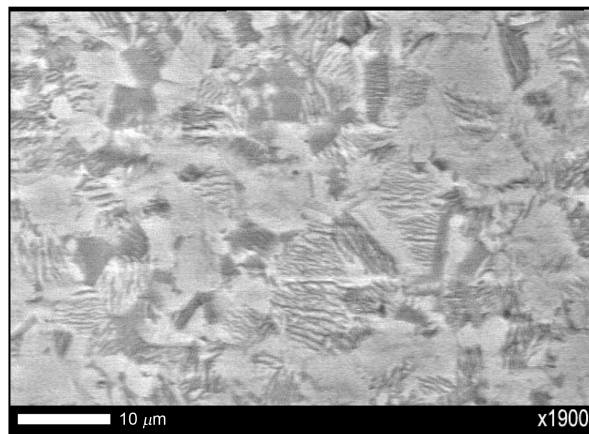

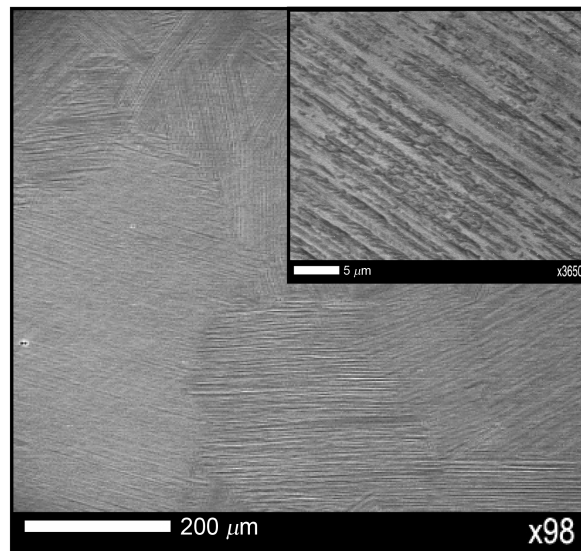Fig. 11 SEM of Ti-48%Al-2%Cr-2%Nb (at%) sample tile T3

Fig. 12 SEM of P^{2}C$^®$ consolidated Ti-48%Al-2%Cr-2%Nb tile T4

The Scanning Electron Microscopy (SEM) micrographs of tile samples T3 and T4 consolidated from Ti-48%Al-2%Cr-2%Nb powders are shown in Figs. 11 and 12. Sample T3 showed a duplex microstructure with equiaxed gamma grains and lamellar colonies (Fig. 11). The average grain size of the consolidated sample as determined from the line-intercept method was 5 μm. Sample T4 showed a fully lamellar microstructure (Fig. 12). The microstructure showed significant grain growth with the grain size ranging from 100 to 2000 μm. The lamellar spacing in sample T4 was found to be 0.5 μm.

3.3 Mechanical tests

The mechanical properties of the consolidated samples were measured by four-point bending tests. The four-point bending tests were performed to determine elastic modulus and flexure strength of bend bars machined from the consolidated samples. The four-point bending tests were also performed on chevron notch bars to yield fracture toughness. Additionally, the four-point bend tests were performed at temperatures up to 950ºC. The diamond Vickers indent test was used to measure the micro-hardness of all the consolidated samples.

The room temperature four-point bending tests were performed on 3 to 5 bend bar samples machined from each consolidated sample. The mechanical property values reported below are an average of the bend bars tested per sample. On some of the four-point bending tests, a strain gage was attached to the side of the bend bar experiencing tension to measure elastic modulus in tension. In some tests, the strain gage data was not available. Hence, for all samples, the elastic modulus in bending was calculated using load versus displacement data from the four-point bending tests. The room temperature mechanical properties for all the samples are summarized in Tables 2 to 4.The stress versus strain plots of all the samples are shown in Fig. 13.

Figs. 13(a) and 13(b) show the four-point bending test results for discs samples consolidated from Ti-50%Al composition powders. In Fig. 13, samples S2 and S3 exhibited similar stiffness except that the flexure strength for sample S3 was lower than that of S2. The consolidation conditions of both the samples were similar with the exception of the pulsing process. Sample S3 was not subjected to the pulsing process during consolidation. The four-point bending results for samples S4 and S5 are shown in Fig. 13(b). The test results show similar stiffness and flexure strength values for both the samples. Samples S4 and S5 were consolidated under similar conditions, except that the powder compact for sample S5 was not subjected to pulsing process before reaching the

Table 2 Room temperature mechanical properties for Ti-50%Al disc samples

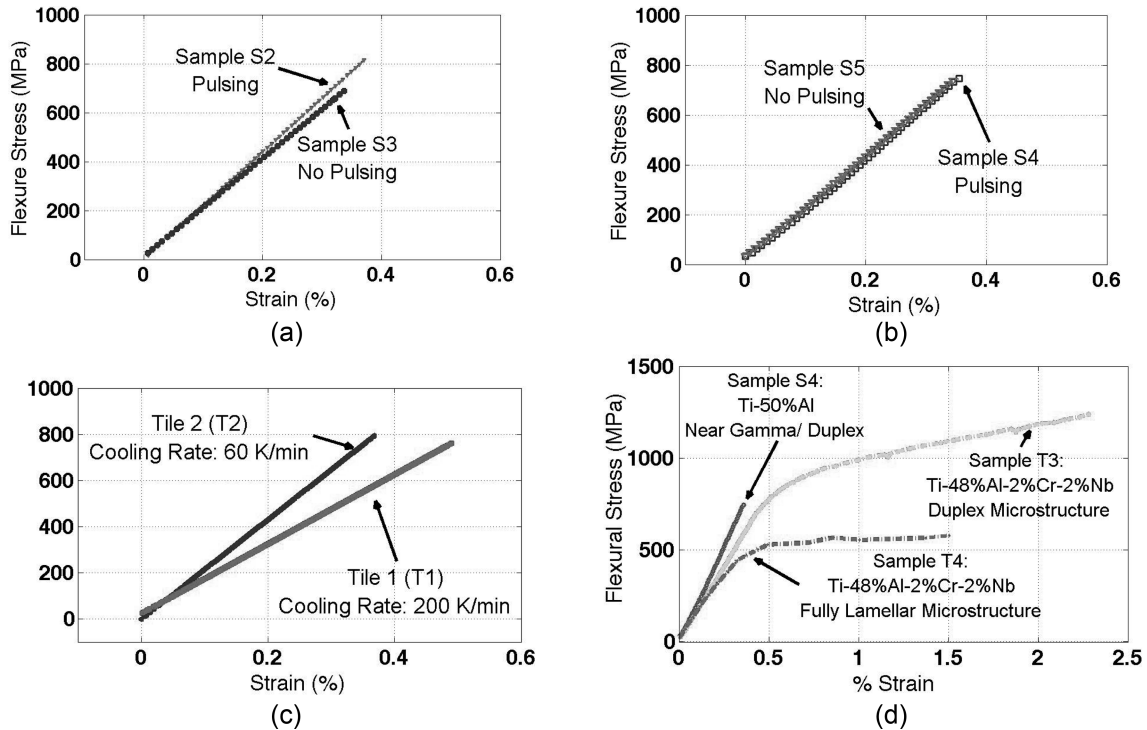| Sample ID	Consolidation temperature (Celsius)	Microstructure type	Flexure strength (MPa)	Elastic modulus in bending (GPa)	Elastic modulus in tension (GPa)	Micro-hardness (GPa)
S1	1200*	Near gamma/Duplex	560.90	130.86	-	2.74
S2	1000*	Near gamma	815.98	149.50	218.98	3.27
S3	1000	Near gamma	691.53	153.94	215.65	3.46
S4	1200*	Near gamma/Duplex	746.54	122.17	206.24	2.84
S5	1200	Near gamma/Duplex	737.33	129.28	206.39	2.83
S6	1400*	Fully Lamellar	422.96	108.12	-	2.58

* Indicates pulsing

Fig. 13 Stress v. Strain plot for samples (a) S2 and S3, (b) S4 and S5, (c) T1 and T2, and (d) T3 and T4 in four-point bending

consolidation temperature.

Fig. 13(c) shows the stress versus strain plot for tiles T1 and T2, which were consolidated from Ti-50%Al composition powder. As shown, the elastic modulus for tile T2 is greater than that of tile T1. Both the tile samples were consolidated under the same conditions except that the cooling rate of tile T2 was accelerated to 200 K/min, while that of tile T1 was set to 60 K/min.

The flexural stress versus strain plots for tiles consolidated from Ti-48%Al-2%Cr-2%Nb powders are shown in Fig. 13(d). Sample T3 with duplex microstructure exhibited a total elongation of 2.3% with 0.5% elastic and 1.8% plastic strain. Sample T4 with a fully lamellar microstructure showed a total elongation of 1.5% with 0.3% elastic and 1.2% plastic strain. For comparison, the flexural stress versus strain plot of Ti-50%Al sample S4 with Near-gamma/Duplex microstructure is also plotted in Fig. 13(d). As shown in the figure, the Ti-50Al alloy composition exhibited no ductility.

The flexural strength, and elastic modulus of all the samples were calculated from the stress versus strain curves in Fig. 13 and are listed in Tables 2 to 4. The fracture toughness values for the tile samples are reported in Table 2 and Table 4. The fracture modes of the consolidated Ti-48%Al-2%Cr-2%Nb specimens T3 and T4 with duplex and fully lamellar microstructure respectively, were determined through microstructural examination of the fractured samples as shown in Figs. 14(a) and 14(b). Sample T3 with duplex microstructure in Fig. 14(a) exhibited transgranular cleavage like fracture, while sample T4 with fully lamellar microstructure exhibited a mix of translamellar and interlamellar mode of fracture as shown in Fig. 14(b).

The high temperature mechanical properties were measured by conducting four-point bending

Table 3 Mechanical properties for Ti-50%Al tiles

Sample	Cooling rate (K/Min)	Modulus in bending (GPa)	Modulus in tension (GPa)	Flexural strength (MPa)	Fracture toughness (MPa m$^{1/2}$)	Micro-hardness (GPa)
T1	200	132.58	148.76	787.60	7.61	2.88
T2	60	151.47	216.23	808.91	9.43	3.23

Table 4 Room temperature mechanical properties of Ti-48%Al-2%Cr-2%Nb samples compared to that of Ti-50%Al samples with similar microstructure type

Sample ID	Micro-structure type	Grain size (mm)	Elongation (%)	Elastic modulus (GPa)	Flexural strength (MPa)	Fracture toughness (MPa m$^{1/2}$)	Micro-hardness (GPa)
T3	Duplex	5	2.3	154.48	1238.62	17.95	2.90
T4	Fully Lamellar	100-2000	1.5	134.59	578.51	-	2.55
S4	Near-gamma/ Duplex	13	0.3	203.90	746.54	9.43	3.46
S6	Fully Lamelar	50-100	-	-	422.96	-	2.58

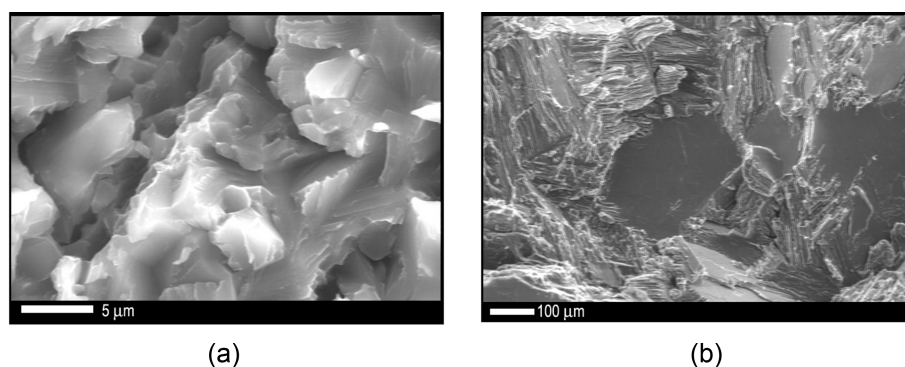(a)   (b)

Fig. 14 SEM of fractured T3 - Ti-48%Al-2%Cr-2%Nb samples with duplex microstructure

tests at temperatures up to 950°C. These tests were conducted on bend bars machined from samples S1, T2 and T3. The high temperature tests for sample S1 were conducted up to 500°C due to the limited number of bend bars available from sample S1 (One-inch diameter disc). The four-point bending fixture was loaded in a MTS test frame and enclosed with a clamshell oven. The plot in Fig. 15(a) shows the force versus displacement curves for sample S1 at high temperatures in air.

The flexure strength and modulus in bending of sample S1 at four different temperatures are tabulated in Table 5. The flexure strength was found to increase with temperature. The modulus in bending also increases with temperature up to 350°C and then starts to decrease. The high temperature mechanical properties for Ti-50%Al tile T2 were characterized at temperatures up to 950°C both in air and vacuum. This was done by conducting four-point bending tests at high temperatures in air and

Table 5 High temperature mechanical properties of Ti-50%Al sample S1 in air

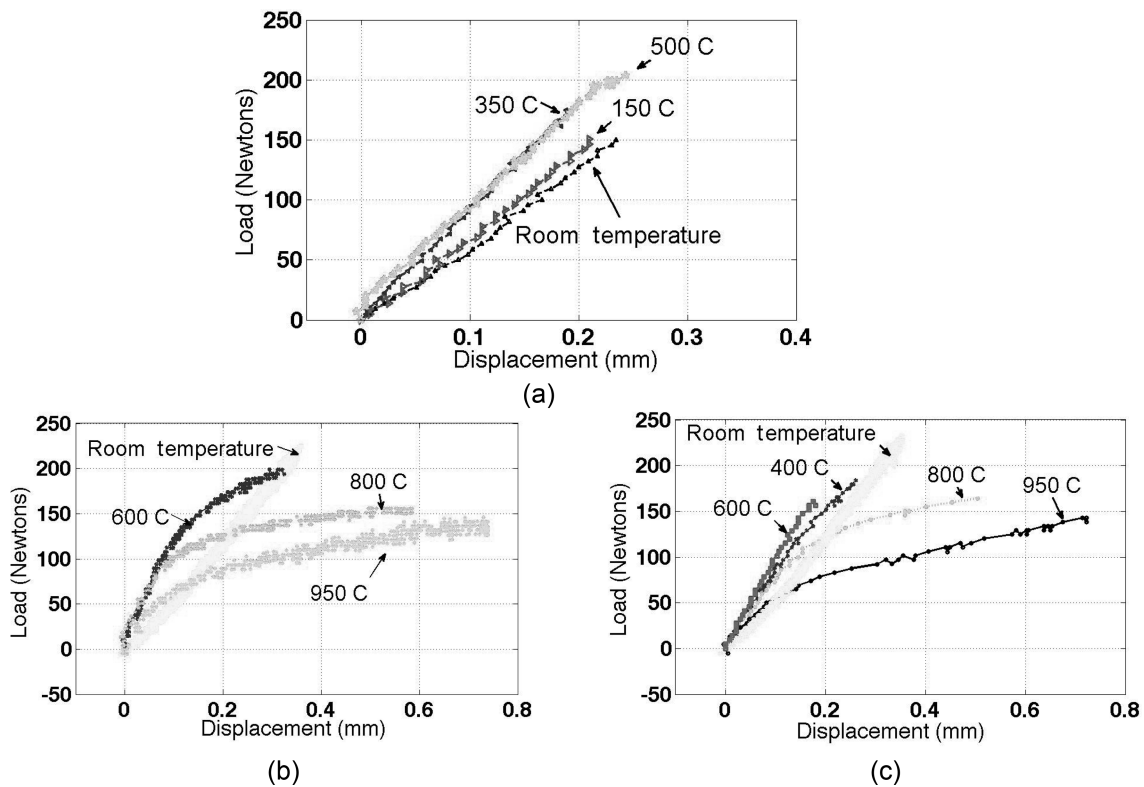| Temperature (Celsius)	Flexural strength (MPa)	Modulus in bending (GPa)
15	560.90	131.04
150	593.96	144.10
350	622.10	183.74
500	806.24	170.12

Fig. 15 High temperature force versus displacement plots showing for (a) sample S1 in air, (b) sample T2 in air and (c) sample T2 in vacuum

vacuum. The force versus displacement plots for high temperature four-point bending tests for tile T2 in air and vacuum are shown in Figs. 15(a) and 15(b), respectively. Fig. 16 further shows the bending modulus profile as a function of temperature for tile T2 in air and vacuum.

As shown in Fig. 17(a), the flexure strength of tile T2 was found to increase with increase in temperature up to 400°C and then started decreasing. The flexure strength at 950°C was found to be 75% of the flexure strength at room temperature. Furthermore, the bending modulus was also found to increase with temperature up to 600°C and then started to decrease. The material exhibited plastic deformation above 600°C.

Fig. 17(b) shows the flexure strength of Ti-48%Al-2%Cr-2%Nb tile T3 samples in air and vacuum at high temperatures. Above 700°C the T3 samples exhibited large elongation. As a result,
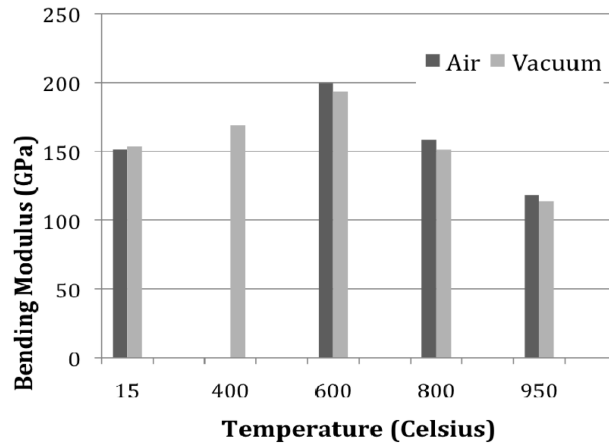
Fig. 16 Bending modulus v. temperature plot for Ti-50%Al sample T2 in air and vacuum

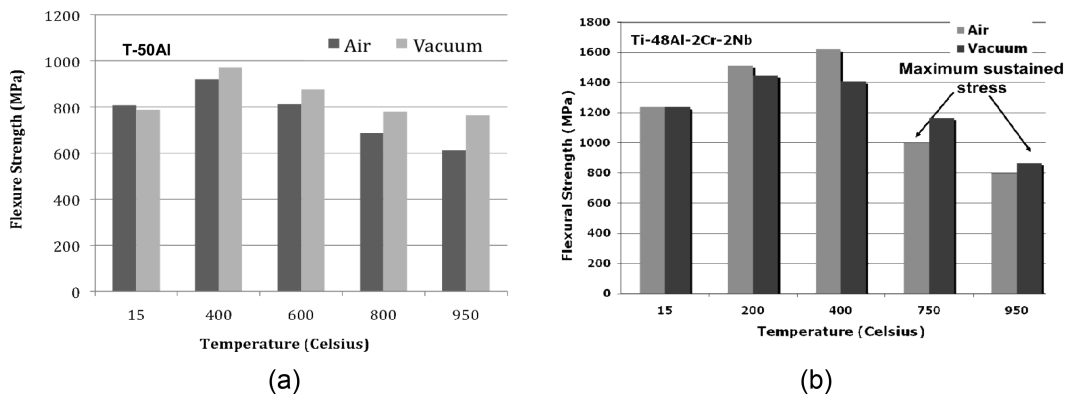(a)   (b)

Fig. 17 High temperature flexural strength for (a) Ti-50%Al sample T2, and (b) Ti-48%Al-2%Cr-2%Nb sample T3 in air and vacuum

T3 samples could not be loaded to failure. The clearance in the four-point bending set-up was insufficient to accommodate the deformation of T3 samples to failure. Thus, the flexural stresses shown for T3 samples above 700°C in Table 7 are the maximum stress values sustained by T3 samples before passing the four-point bending fixture clearance. They do not reflect their failure stresses.

3.4 Comparison to State-of-the-Art

The ultimate tensile strength of γ-TiAl alloys have usually been reported in the range of 400-700 MPa (Kim 1989, Kim and Dimiduk 1991, Schafrik 1977, Lipsitt 1975) but a direct comparison cannot be made with these values since the values reported in the present work are flexural strengths. The room temperature flexural strength of T3 samples with duplex microstructure was found to be 30% superior to that of TiAl alloys consolidated via a similar pulse discharge sintering process (Sun and Hashimoto 2003). Ductility was comparable to that of γ-MET TiAl alloys consolidated via HIP

(Draper *et al.* 2003). Fracture toughness of ~18 MPa m$^{1/2}$ was also superior to that of duplex micro-structured TiAl alloys with fracture toughness in the range of 12-15 MPa m$^{1/2}$. Similarly, sample T4 with a fully lamellar microstructure exhibited 40% more ductility than that of fully lamellar TiAl alloys (Kim 1989, Draper *et al.* 2003, Srivatsan *et al.* 1995). The microhardness value for sample T3 was found to be 20% lower than the Vickers hardness of γ-MET TiAl alloys consolidated via HIP (Draper *et al.* 2003), but was comparable to that of as-cast base Ti-48%Al (Adams *et al.* 1990).

4. Discussion

4.1 Microstructural evolution

Ti-50%Al and Ti-48%Al-2%Cr-2%Nb powders were consolidated in the $\alpha_2+\gamma$, $\alpha+\gamma$, and pure α phase fields as shown in the Ti-Al binary phase diagram in Fig. 5. As a result, three characteristic microstructures were produced, namely (1) near gamma, (2) duplex, and (3) fully lamellar.

Near Gamma Microstructure – Samples S2, S3, T1 and T2: Near gamma microstructure was obtained in samples S2 and S3, which were consolidated in the $\alpha_2+\gamma$ phase field at T_α - 435°C (1000°C). The gamma phase is the dominant phase at this composition. Therefore, heat-treatment at these temperatures results in the formation of coarse gamma grains (Sun 1999). But due to the reduced consolidation time, grain growth was controlled in both the samples, which led to the formation of fine gamma grains characterized with continuous bands of segregated α_2-Ti$_3$Al particles at the grain boundaries as shown in Fig. 19(a).

The microstructure for samples T1 and T2 showed characteristics of near gamma microstructure, except that it consisted of a significant amount of pores segregated at the grain boundaries. This can be attributed to the fact that T1 and T2 were tile samples, which were much larger in size than the disc samples. The consolidation time for the tiles was only 15 to 20 minutes, while that of the discs was 10 minutes. Comparing the ratios of the size of the disc to size of the tile to that of their consolidation times it is evident that consolidation time of the tiles was not long enough. This is further apparent in the density values obtained for the tiles. The density of the tiles was much lower than the density of both the α_2 and γ phases.

Duplex Microstructure – Samples S1, S4, S5, and T3: Samples S1, S4, S5, and T3 were consolidated in the $\alpha+\gamma$ phase fields at 1200°C. Samples T3 and T4 as listed in Table 1 have an alloy composition with small additions of Cr and Nb. Due to these additions, the phase boundaries of these samples were shifted such that the alloy behaved as if it had less Al concentration (Rivard 2005). As a result, the alpha-transus line was shifted to the right as indicated by the dotted line in Fig. 5, and the effective alpha-transus temperature was less than that of Ti-50Al alloy in samples S1, S4 and S5. This explains that, although Ti-50Al samples S1, S4, S5 and Ti-48%Al-2%Cr-2%Nb sample T3 were consolidated at the same temperature (1200°C), the T3 sample microstructure was different than that of S1, S4, and S5 as shown in Fig. 7, Fig. 9(c-d), and Fig. 11.

At 1200°C samples S1, S4 and S5 are at T_α - 235°C, while sample T3 was at T_α - 145°C. The consolidation temperature of sample T3 was therefore closer to T_a than that of samples S1, S4, and S5. At T_α - 145°C, sample T3 was in a phase field where the volume fractions of gamma phase and alpha phase are approximately equal. At this state, the formation of the alpha phase becomes prominent. The initially dominant gamma phase is gradually reduced in volume until an equilibrium volume fraction is reached and grain growth occurs. The growth of grains, however, is limited by

the dispersed alpha phase, which also grows. These competitive growth processes lead to a formation of fine mixture of lamellar colonies and gamma grains resulting in a duplex microstructure as shown in Fig. 11.

At T_α - 235ºC, below the α_2/γ equilibrium temperature gamma phase is dominant but the α_2 phase is present in significant volumes. The α_2 particles start disordering at this temperature, and alpha precipitates begin nucleating to grow into alpha plates resulting in the formation of lamellar colonies. The formation of the lamellar colonies is further characterized by grain growth. At T_α - 235ºC, the alpha precipitates, which do not form lamellar colonies remain segregated at the grain boundaries. The gamma phase at this temperature forms a mix of coarse and fine gamma grains. Hence, the resulting microstructure is a mix of large and fine gamma grains with lamellar colonies. This microstructure has been termed as a combination of Near gamma and Duplex. The Duplex microstructure is usually characterized with fine gamma grains and lamellar colonies. But in this case, the large gamma grains are still present while the lamellar colonies are growing. The growth of gamma grains and lamellar colonies has not reached an equilibrium. Hence, we see a mix of large gamma grains, as well as fine gamma grains along with growing lamellar colonies.

As discussed earlier, the duplex microstructure is characterized by fine gamma grains and lamellar colonies. Hence the grain size in the duplex microstructure is found to be the lowest. The grain size in sample T3 with duplex microstructure was found to be 5 μm. The grain size for samples S1, S4 and S5 was found to be 20 μm, 13 μm, and 13 μm, respectively. The consolidation time for sample S1 was 20 minutes, while that of S4 and S5 was 10 minutes. The effect of higher consolidation time for sample S1 is evident in the increase in average grain size.

Fully Lamellar Microstructure – Samples S6 & T4: Sample S6 was consolidated at T_α - 45ºC. At this temperature, the α phase is the dominant phase. Hence, consolidation at this temperature results in the formation of lamellar colonies. Since, the volume fraction of the gamma phase is small compared to that of alpha phase, the formation of lamellar colonies is very rapid. There are no barriers restricting the growth of lamellar colonies and the resultant colony size is much larger than for the samples consolidated at lower temperatures. The average colony size for sample S6 was found to be in the range of 75 μm.

Sample T4 was consolidated at T_α + 55ºC in the pure alpha field, which resulted in the formation of fully lamellar microstructure with large lamellar grains (Prasad and Chaturvedi 2004) as shown in Fig. 12. The grain growth at temperatures above T_α is high due to the fast diffusivity of the alloy constituents. Therefore, even rapid consolidation at such high temperatures cannot control grain growth in sample T4.

Sample S6, which was consolidated at the same temperature as sample T4 did not exhibit extreme rapid grain growth as sample T4. As shown in Fig. 9(e), the grain size of sample S6 is between 50μm to 100 μm, while that of sample T4 is between 100 μm-2000 μm. This is due to the fact that the alpha-transus temperature of sample T4 was lowered due to small additions of Nb and Cr. Hence, with reference to the T_a temperature, sample T4 was consolidated at T_α + 55ºC in pure alpha phase field, while sample S6 was consolidated at T_α - 35ºC still in the $\alpha + \gamma$ phase field but very close to the alpha-transus line. The presence of γ phase impeded extreme rapid grain growth in sample S6.

4.2 Factors affecting mechanical properties

Microstructure and Grain Size: As evident from the previous section, each microstructure is characterized by a particular grain size and morphology. In order to confirm the Hall-Petch
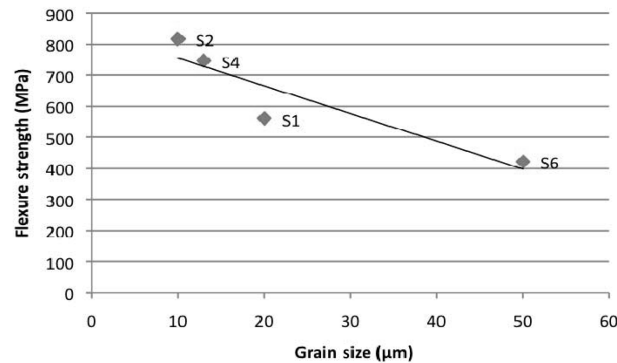
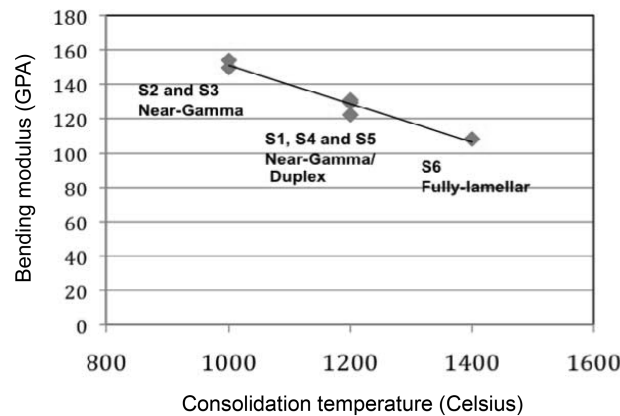Fig. 18 Flexural strength of Ti-50%Al disc samples v. grain size

Fig. 19 Effect of microstructure morphology on bending modulus of Ti-50%Al samples S1 through S6

relationship between grain size and strength, the flexure strengths of samples S1, S2, S4 and S6 were compared. For consistency in comparison, all the samples chosen for comparison are disc samples of Ti-50%Al composition. These disc samples were applied with a pulsed DC voltage before consolidation. The mechanical properties and grain size of the four samples chosen for comparison are listed in Table 2. A plot of flexure strength versus grain size in Fig. 18 shows the inverse relationship between the grain size and flexure strength.

Further from Table 2, it can be concluded that the elastic modulus in bending is dependent on the microstructural morphology. For microstructure with dominant gamma phase such as Near gamma, the elastic modulus in bending is highest and steadily decreases for Near gamma/Duplex and Fully lamellar as the volume fraction of gamma phase decreases and α_2 phase increases. This is evident in Fig. 19, where the bending modulus of disc samples S1 through S6 (with Ti-50%Al composition) is plotted against its consolidation temperatures. This can be attributed to the fact that the elastic modulus for α_2 (Ti$_3$Al) is in the range of 110 GPa, while that of γ (TiAl) is in the range of 180 GPa (Sauthoff 1995).

The same relationship holds for micro-hardness of the material. As evident from Table 2 and Fig. 20, the micro-hardness of samples exhibiting Near gamma microstructure is high and steadily
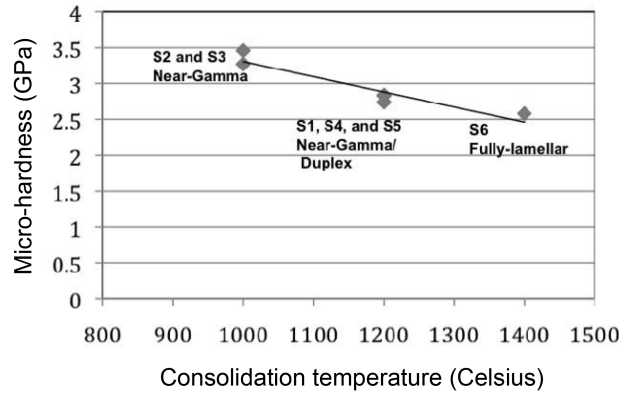
Fig. 20 Effect of microstructure morphology on micro-hardness of Ti-50%Al disc samples S1 through S6

decreases for Near gamma/Duplex and Fully lamellar with increasing α_2 (Ti$_3$Al) phase.

Pulsing: For comparison purposes, two of the disc samples S3 and S5 were not subjected to a pulsed DC voltage before consolidation. As discussed earlier, pulsing removes all oxides and other impurities from the surface of the powders. This in turn enhances particle rearrangement and diffusion.

Pulsing had significant impact on the samples consolidated at temperature (1000°C) in the $\alpha_2 + \gamma$ phase field. As evident from comparison of microstructures of samples S2 (Fig. 9(a)) and S3 (Fig. 9(b)), sample S3 (not applied with the pulsing process) showed increased presence of Oxygen and Carbon compared to that of sample S2 (applied with the pulsing process). Furthermore, the flexural strength of S3 (~691 MPa) was significantly lower than that of S2 (~815 MPa). These comparisons show that the pulsing process enhanced diffusion in sample S2 and as a result there were minimal amount of impurities present in the sample. This in turn enhanced its flexure strength.

On the other hand, pulsing did not play a significant role in enhancing diffusion at higher temperatures. Samples S4 and S5 were consolidated in the $\alpha_2 + \gamma$ phase field at 1200°C. Sample S4 was subjected to the pulsing process, while S5 was not. The microstructures of both the samples S4 (Fig. 9(c)) and S5 (Fig. 9(d)) were similar except that the microstructure of sample S5 had small traces of Oxygen and Carbon at the grain boundaries. The flexure strengths of both the samples were also in the same range (S4: ~746 MPa and S5: ~737 MPa). This can be attributed to the fact that diffusion is usually enhanced at higher temperatures. Hence, application of the pulsing process did not play a significant role in enhancing diffusion for samples consolidated at or above temperatures in the $\alpha + \gamma$ phase field.

Cooling Rate: The rate at which a γ-TiAl is cooled after heat-treatment has been reported to play a role in its microstructure and mechanical properties (Sun 1999). Hence, the two tiles consolidated from Ti-50%Al powders were subjected to different cooling rates after the consolidation process. Tile 1 (T1) was cooled at 200 K/min, while Tile 2 (T2) was cooled at 60 K/min. Both the tiles were consolidated at 1000°C in the $\alpha_2 + \gamma$ phase field. Rapid cooling from the consolidation temperature freezes the high temperature phase (α_2 phase) in the consolidated sample. This in turn increases the α_2 volume fraction. One of the effects of the increase in the α_2 volume fraction is decrease in the stiffness of the material. This is due to the fact that α_2 (Ti$_3$Al) phase has an elastic modulus in the range of 110 GPa, while the γ (TiAl) phase has an elastic modulus in the range of 180 GPa. As

shown in Table 3 and Fig. 13(c), the elastic modulus of T1 is approximately 150 GPa, while that of T2 is approximately 215 GPa. This difference is due to the rapid cooling of T1, which in turn retained a high volume fraction of the α_2 phase.

Alloy Composition: γ-TiAl has been reported to have maximum ductility for Ti-48%Al composition (Kim 1991, Sauthoff 1995, Froes and Suryanarayana 1995). The decreased ductility with increasing aluminum content is attributed to increased tetragonality ratio or decreased metallic bonding (Simpkins *et al.* 2007). Addition of Cr increases metallic bonding by decreasing aluminum content in the gamma phase (Cerreta and Mahajan 2001). Therefore, T3 samples with 48%Al and 2%Cr and Duplex microstructure exhibited the maximum ductility. Ti-48%Al-2%Cr-2%Nb sample T4 with fully lamellar microstructure exhibited significantly higher ductility than Ti-50%Al sample S6 (with fully lamellar microstructure). Although, both samples had similar microstructures, the addition of Cr and alloy composition in the Ti-48%Al range increased ductility in sample T4.

Similarly T3 samples with Ti-48%Al-2%Cr-2%Nb composition and Duplex microstructure also exhibited ductility and fracture toughness higher than sample S4 with Ti-50%Al composition and Near gamma/Duplex microstructure as shown in Table 4. The addition of Nb is known to increase strength as well as fracture toughness in gamma titanium aluminides (Kim 1995) as evident in Table 4.

4.3 High temperature mechanical properties

Dependence of Flexure Strength and Elastic Modulus on High Temperature: Gamma titanium aluminides have been found to exhibit anomalous mechanical behavior at high temperatures. The tensile stress of gamma titanium aluminides has been found to increase with temperature up to 400°C.

The $P^2C^{®}$ consolidated samples S2, T2, and T3 exhibited anomalous mechanical behavior at high temperature. This can be seen in flexure strength versus temperature plots for samples T2 and T3 in Fig. 17. The elastic modulus in bending was also found to increase with temperature up to 600°C. At temperatures below 600°C, any metastable $\alpha_2 + \gamma$ phase present in the material transforms into pure γ phase. Since, the elastic modulus of γ phase is higher than that of α_2 phase, the elastic modulus is found to increase with temperature up to 600°C. Between 600°C and 700°C, the material goes through its glass transition temperature and hence it shows reduction in its stiffness.

Effect of Atmosphere on Strength at High Temperature: In order to study the effects of high temperature exposure in air to the mechanical properties of Ti-50%Al, sample T2 was tested for mechanical properties in air and vacuum. As seen in Fig. 17, the flexure strength of sample T2 in air at high temperatures was found to be 10% lower than the flexure strength in vacuum. This indicates that high temperature exposure in air has an adverse effect on the flexure strength of titanium aluminides with Ti-50%Al composition.

As mentioned earlier, the Ti-48Al-2Nb-2Cr sample T3 was tested at high temperatures in air and vacuum. The T3 samples tested above 600°C could not be loaded to failure due to the enormous elongation it exhibited above 600°C. Hence, the data points above 600°C in Fig. 17(b) report the maximum stress sustained by the samples before passing the four-point bending fixture clearance. At temperatures below 600°C, the T3 samples exhibited approximately equal if not better strength in air than in vacuum. This could be attributed to the presence of Nb, which impedes absorption of Oxygen and hence protects against embrittlement and thereby premature fracture (Woo *et al.* 2003).

5. Conclusions

1. Micron-sized γ-TiAl powders of Ti-50%Al and Ti-48%Nb-2%Cr-2%Nb (at%) composition powders were consolidated by $P^2C^®$ to produce fully dense near-net shape parts in the form of 0.25 inch thick, 1" diameter discs and 3" × 2.5" dimension tiles. The microstructure of the consolidated samples revealed minimal grain growth and thereby exhibited enhanced mechanical performance. Parameters to consolidate γ-TiAl samples by $P^2C^®$ were chosen using the Ti-Al binary phase diagram. Three characteristic microstructures namely Near-Gamma, Duplex, and Fully Lamellar were produced in the $P^2C^®$ consolidated γ-TiAl samples.

2. A correlation between the consolidation parameters and microstructural morphology was established. The mechanical properties of consolidated γ-TiAl samples were characterized and a relationship between the microstructural morphology and mechanical properties was established. The mechanical properties were found to depend strongly on the microstructure morphology, grain size and alloy composition. γ-TiAl alloy with Ti-48%Al-2%Cr-2%Nb composition and duplex microstructure was found to exhibit the best set of mechanical properties.

3. The presence of impurities in powders usually creates a diffusion barrier during consolidation process. Hence, a pulsed DC voltage was applied to the powder compact during the consolidation of γ-TiAl samples. The pulsing of the voltage through the powder compact charges the powder particles relative to each other and leads to generation of sparks or plasma. The formation of plasma removes the diffusion barrier that comprises of oxides and other contaminants. This was evident for samples consolidated at 1000ºC. For samples consolidated at higher temperatures (>1200ºC), the effect of pulsing was not apparent.

4. The effect of cooling rate (during the cooling cycle of the consolidation process) on the mechanical properties of Ti-50%Al was examined. Rapid cooling from the consolidation temperature freezes the high temperature phase (α_2 phase) in the consolidated sample. This in turn increases the α_2 volume fraction. The increase in the α_2 volume fraction decreases the stiffness of the material.

5. The mechanical behavior of the consolidated γ-TiAl parts was characterized at temperatures up to 1000ºC. γ-TiAl samples exhibited increase in flexure strength up to 500ºC due to microstructure refinement. The bending modulus was found to increase with increase in temperature up to 600ºC due to phase transformation of the $\alpha_2 + \gamma$ metastable phase in to pure γ phase. Exposure to air at high temperatures resulted in deterioration of the flexure strength of Ti-50%Al samples by 10%.

6. Small additions of Nb and Cr (in the order of 2at%) along with a small decrease in Aluminum concentration (from 50at% to 48at%) resulted in a significant change in the mechanical behavior of the consolidated titanium aluminide parts. Consolidation of titanium aluminide powders with a composition of Ti-48%Al-2%Nb-2%Cr resulted in formation of titanium aluminide parts with superior room temperature ductility, and high temperature strength.

References

Adams, L., Kampe, S. and Christodoulou, L. (1990), "Characterization of rapidly solidified ceramic-titanium aluminide powders", *Int. J. Powder Metall.*, **26**(2), 105-114.

Appel, F., Oehring, M. and Wagner, R. (2000), "Novel design concepts for gamma-based titanium alumnide alloys", *Intermetallics*, **8**(9-11), 1283-1312.

ASTM, (1997), *Annual Book of ASTM Standards*, American Society for Testing and Materials, West Conshohocken, PA.

Cerreta, E. and Mahajan, S. (2001), "Formation of deformation twins in TiAl", *Acta Mater.*, **49**(18), 3803-3809.

Cheng, T. and McLean, M. (1997), "Characterization of TiAl intermetallic rods produced from elemental powders by hot extrusion reaction synthesis (HERS)", *J. Mater. Sci.*, **32**(23), 6255-6261.

Chen, Y.Y., Yua, H.B., Zhang, D.L. and Chaia L.H. (2009), "Effect of spark plasma sintering temperature on microstructure and mechanical properties of an ultrafine grained TiAl intermetallic alloy", *Mater. Sci. Eng.: A.*, **525**, 166-173.

Christop, U., Appel, F. and Wagner, R. (1997), "High-temperature ordered intermetallic alloys VII", *Mater. Res. Sot. Symp. Proc.,* Pittsburgh, **460**, 207-212.

Das, G., Kestler, H. Clemens, H., and Bartolotta, P.A. (2004), "Sheet gamma TiAl: status and opportunities", *J. Mater.*, **56**(11), 42-45.

Djanarthany, S., Viala, J.C. and Bouix, J. (2001), "An overview of monolithic titanium aluminides based on Ti_3Al and TiAl", *Mater. Chem. Phys.*, **72**(3), 301-319.

Draper, L.S. Das, G. Locci, I. Whittenberger, J.D. Lerch, B.A. and Kestler, H. (Ed.) (2003), *Gamma Titanium Aluminides,* Kim, Y.W. Helmut, C. and Rosenberger, A.H., TMS, PA.

Froes, F.H., Suryanarayana, C. and Eliezer, D. (1992), *"*Review synthesis, properties and applications of titanium aluminides", *J. Mater. Sci.*, **27**(19), 5113-5140.

Froes, F.H. and Suryanarayana, C. (1995), *Phys. Metal. Process. Intermetallics Compounds.* Chapman and Hall, NY.

Fu, E., Rawlings, R.D. and McShane, H.B. (2001), "Reaction synthesis of titanium aluminides", *J. Mater. Sci.*, **36**(23), 5537-5542.

Gerling, R., Bartels, A. and Clemens, H. (2004), "Structural characterization and tensile properties of a high Nb containing gamma TiAl sheet obtained by powder metallurgical processing", *Intermetallics*, **12**(3), 275-280.

Hibbeler, R.C. (1997), *Mech. Mater.* 3rd Edition, Prentice Hall, Upper Saddle River, NJ.

Hitoshi, H. and Sun, Z. (2003), "Fabrication of TiAl alloys by MA-PDS process and the mechanical properties", *Intermetallics*, **11**(8), 825-834.

Immarigeon, J.P., Holt, R.T., Koul, A.K., Zhao, L., Wallace, L. and Beddoes, J.C. (1995), "Lightweight materials for aircraft applications", *Mater. Charect.*, **35**(1), 41-67.

Kim*,* Y.W. (1989), "Intermetallic alloys based on gamma titanium aluminides", *J. Mater.,* **41**(7)*,* 24-30.

Kim, Y.W. (1991), "Microstructural evolution and mechanical properties of a forged gamma titanium alloy", *Acta Metall. Mater.*, **40**(6), 1121-1133.

Kim, Y.W. (1995), "Effects of microstructure on the deformation and fracture of gamma-TiAl alloys", *Mater. Sci. Eng.*, **Al92/193**, 519-533.

Kim, Y.W. (1998), "Strength and ductility in TiAl alloys", *Intermetallics*, **6**(7-8), 623-628.

Kim, Y.W. and Dimiduk, D. (1991), "Progress in the understanding of gamma titanium aluminides", *JOM*, **43**(8), 40-47.

Krause, P., Bartolotta, A. and David, L. (1999), "Titanium aluminide applications in the high speed civil transport", *Proceedings of International Symposium on Gamma Titanium Aluminides*, CA, USA.

Lipsitt, H.A. (1975), "The deformation and fracture of TiAl at elevated temperatures", *Metall. Mater. Trans. A*, **6**(11), 1991-1996.

Lu, X., He, X.B., Zhang, B., Zhang, L., Qu, X.H. and Guo, Z.X. (2009), "Microstructure and mechanical properties of a spark plasma sintered Ti–45Al–8.5Nb–0.2W–0.2B–0.1Y alloy", *Intermetallics*, **17**(10), 840-846.

Marketz, W.T., Fischer, F.D., Kauffmann, F., Dehm, G., Bidlingmaier, T., Wanner, A. and Clemens, H. (2002), "On the role of twinning during room temperature deformation of gamma-TiAl based alloys", *Mater. Sci. Eng.*, **331**, 177-183.

Prasad, U. and Chaturvedi, M.C. (2004), "Grain coarsening in Ti–45Al based titanium aluminides at supertransus temperature and subsequent lamellar structure formation", *Mater. Sci. Tech.*, **20**(1), 87-92.

Rivard, J. (2005), "Development of a finite volume model for the high-density infrared processing of gamma-TiAl thin-gage sheet", *PhD Thesis*, University of Cincinnati, Cincinnati, OH.

Sahay, S.S., Ravichandran, K.S., Atri, R., Chen, B. and Rubin, J. (1999), "Evolution of microstructure and

phases in in-situ processed Ti-TiB composites containing high volume fractions of TiB whiskers", *J. Mater. Res.*, **14**(11), 4214-4221.

Sauthoff, G. (1995), *Intermetallics*, Wiley-VCH, Weinheim, New York.

Schafrik, R.E. (1977), "Dynamic elastic moduli of titanium aluminides", *Metall. Trans. A.*, **8**(6), 1003-1006.

Shazly, M., Prakash, V. and Draper, S. (2009), "Dynamic fracture initiation toughness of a gamma (Met-PX) titanium aluminide at elevated temperatures", *Metall. Mater. Trans. A.*, **40**(6), 1400-1412.

Simpkins, R., Rourke, M., Bieler, T. and McQuay, P.A. (2007), "The effects of HIP pore closure and age hardening on primary creep and tensile property variations in a TiAl XD^TM alloy with 0.1 wt.% carbon", *Mater. Sci. Eng.*, **463**(1-2), 208-215.

Soboyejo, W.O., Ye, F. and Srivatsan, T.S. (1997), "The fatigue and fracture behavior of a gamma-titanium alumnide intermtallic: Influence of ductile phase reinforcement", *Eng. Fract. Mech.*, **56**(3), 379-395.

Soboyejo, W.O., Shen, W., Lou, J., Mercer, C., Sinha, V. and Soboyejo, A.B.O. (2004), "Probabilistic framework for the modeling of fatigue in cast lamellar gamma-based titanium aluminides", *Mech. Mater.*, **36**(1-2), 177-197.

Sommer, A.W. and Keijzers, G.C. (Ed.) (2003), *Gamma Titanium Aluminides*, Y.W. Kim, H. Clemens and A.H. Rosenberger, TMS, PA.

Srivatsan, T.S., Soboyejo, W.O. and Strangwood, M. (1995). "Cyclic fatigue and fracture behavior of a gamma-titanium aluminide intermetallic", *Eng. Fract. Mech.*, **52**(1), 107-120.

Sun, Y.Q. (1999). *Gamma Titanium Aluminides*. [Edition] Kim, Y.W., TMS, PA.

Sun, Z. and Hashimoto, H. (2003), "Fabrication of TiAl alloys by MA-PDS process and the mechanical properties", *Intermetallics*, **11**(8), 823-834.

Szewczak, E., Paszula, J., Leonov, A.V. and Matyja, H. (1997), "Explosive consolidation of mechanically alloyed Ti-Al alloys", *Mater. Sci. Eng. A.*, **226/228**(15), 115-118.

Voice, W. (1999), "The future of gamma-titanium alumnides by rolls royce", *Aircr. Eng. Aerosp. Tech.*, **71**(4), 337-340.

Voice, W., Henderson, M., Shelton, E. and Wu, X. (2005), "Gamma titanium aluminide, TNB", *Intermetallics*, **13**(9), 959-964.

Woo, J.C., Varma, S.K. and Mahapatra, R.N. (2003), "Oxidation behavior and transmission electron microscope characterization of Ti-44Al-xNb-2(Ta,Zr) alloys", *Metall. Mater. Trans. A*, **34**(10), 2263-2271.

Yolton, C.F. Kim, Y.W. and Habel, U. (Ed.) (2003), *Gamma Titanium Aluminides*, Kim, Y.W., Helmut, C. and Rosenberger, A.H., TMS, PA.

Zhang, W., Liu, Y., Liu, B. and Huang, B.Y. (2011), "Comparative assessment of microstructure and compressive behaviours of PM TiAl alloy prepared by HIP and Pseudo-HIP technology", *Powder Metall.*, **54**(2), 133-141.